AFGL-TR-88-0220

Global Density Specification in the Lower Thermosphere

Jeffrey M. Forbes

Boston University
Center for Space Physics and
Department of Electrical, Computer,
and Systems Engineering
Boston, MA 02215

31 August 1988

Final Report
Period Covered: 15 June 1985 to 17 June 1988

AIR FORCE GEOPHYSICS LABORATORY
AIR FORCE SYSTEMS COMMAND
UNITED STATES AIR FORCE
HANSCOM AIR FORCE BASE, MASSACHUSETTS 01731-5000

"This technical report has been reviewed and is approved for publication"

FRANK A. MARCOS
Contract Manager

WILLIAM K. VICKERY
Acting Branch Chief

FOR THE COMMANDER

ROBERT A. SKRIVANEK
Division Director

This report has been reviewed by the ESD Public Affairs Office (PA) and is releasable to the National Technical Information Service (NTIS).

Qualified requestors may obtain additional copies from Defense Technical Information Center. All others should apply to the National Technical Information Service.

If your address has changed, or if you wish to be removed from the mailing list, or if the addressee is no longer employed by your organization, please notify AFGL/DAA, Hanscom AFB, MA 01731. This will assist us in maintaining current mailing list.

Do not return copies of this report unless contractual obligations or notice on a specific document requires that it be returned.

Unclassified
SECURITY CLASSIFICATION OF THIS PAGE

REPORT DOCUMENTATION PAGE

1a. REPORT SECURITY CLASSIFICATION: Unclassified	1b. RESTRICTIVE MARKINGS
2a. SECURITY CLASSIFICATION AUTHORITY	3. DISTRIBUTION / AVAILABILITY OF REPORT: Approved for public release; Distribution unlimited
2b. DECLASSIFICATION / DOWNGRADING SCHEDULE	
4. PERFORMING ORGANIZATION REPORT NUMBER(S)	5. MONITORING ORGANIZATION REPORT NUMBER(S): AFGL-TR-88-0220
6a. NAME OF PERFORMING ORGANIZATION: Boston University; 6b. OFFICE SYMBOL (If applicable)	7a. NAME OF MONITORING ORGANIZATION: Air Force Geophysics Laboratory
6c. ADDRESS (City, State, and ZIP Code): Ctr for Space Physics & Dept of Electrical, Computer, and Systems Engineering, Boston, MA 02215	7b. ADDRESS (City, State, and ZIP Code): Hanscom AFB, MA 01731
8a. NAME OF FUNDING / SPONSORING ORGANIZATION: AFGL; 8b. OFFICE SYMBOL (If applicable): LI	9. PROCUREMENT INSTRUMENT IDENTIFICATION NUMBER: F19628-85-K-0041
8c. ADDRESS (City, State, and ZIP Code): Hanscom AFB, MA	10. SOURCE OF FUNDING NUMBERS: PROGRAM ELEMENT NO. 62101F; PROJECT NO. ILIR; TASK NO. 5K; WORK UNIT ACCESSION NO. AA

11. TITLE (Include Security Classification)
Global Density Specification in the Lower Thermosphere (U)

12. PERSONAL AUTHOR(S)
Jeffrey M. Forbes

13a. TYPE OF REPORT	13b. TIME COVERED	14. DATE OF REPORT (Year, Month, Day)	15. PAGE COUNT
Final	FROM 6/15/85 TO 6/17/88	31 August 1988	22

16. SUPPLEMENTARY NOTATION

17. COSATI CODES		
FIELD	GROUP	SUB-GROUP

18. SUBJECT TERMS (Continue on reverse if necessary and identify by block number)
Density; Thermosphere; Winds; Waves; Magnetic Activity; (HO)

19. ABSTRACT (Continue on reverse if necessary and identify by block number)

(1) Energetic inputs were derived from various satellite measurements and ground-based sensors for input into the Thermosphere General Circulation Model (TGCM) simulation of the magnetic storm ocurring on March 22, 1979. The simulation was compared with thermospheric densities and winds measured from an Air Force satellite, and incoherent scatter radar measurements of thermospheric temperatures. An evaluation of the overall performance of the model and various physical processes accounting for discrepancies with the data was performed.
(2) A FORTRAN program was developed to perform wave/spectral analyses of density data from the Satellite Electrostatic Triaxial Accelerometer (SETA) instrument using the maximum entropy method. The program was applied to a subset of available SETA data to illustrate typical wave characteristics for geomagnetically quiet and disturbed conditions.
(3) A climatological summary was performed of the average magnetic activity dependences of high-latitude thermospheric winds and densities below 200 km using SETA data from the March/April, 1979, period. Keywords: (

20. DISTRIBUTION / AVAILABILITY OF ABSTRACT	21. ABSTRACT SECURITY CLASSIFICATION
☐ UNCLASSIFIED/UNLIMITED ☒ SAME AS RPT. ☐ DTIC USERS	Unclassified

22a. NAME OF RESPONSIBLE INDIVIDUAL	22b. TELEPHONE (Include Area Code)	22c. OFFICE SYMBOL
Frank Marcos		AFGL/LIS

DD FORM 1473, 84 MAR — 83 APR edition may be used until exhausted. All other editions are obsolete.

SECURITY CLASSIFICATION OF THIS PAGE
Unclassified

Contents

FIGURE CAPTIONS

Figure 1. Black-white photocopy of color figures displaying bin-averaged (a) daytime (approx. 1030 LT) cross-track wind (positive eastward) component, (b) nighttime (approx. 2130 LT) cross-track wind component, (c) daytime density, and (d) nighttime density, plotted vs. geomagnetic latitude (45-90 degrees) and Kp*, the Kp-index averaged for the 3-hour period containing the measurement with that of the previous 3-hour period.

Figure 2. Line plots of bin-averaged cross-track winds vs. geomagnetic latitude for dayside and nightside for low and high levels of magnetic activity.

Figure 3. Bin-averaged densities normalized to 200 km vs. Kp* for three latitude bins.

Figure 4. Bin-averaged nighttime cross-track winds for two latitude bins vs. several geophysical/geomagnetic indices.

Figure 5. Dayside and nightside cross-track winds for the 3 latitude bins vs. average Kp.

Figure 6. Dayside and nightside cross-track winds for the 3 latitude bins vs. average cross-cap potential.

1. INTRODUCTION

Efforts under Contract F19628-85-k-0041 primarily fell into three categories: (1) Simulation of the thermospheric response to the magnetic storm occurring on March 22, 1979, commonly referred to as the CDAW-6 interval, and an analysis and interpretation of winds and densities observed by the SETA instrument during that period; (2) Development of a FORTRAN program to perform wave/spectral analyses of SETA density data, and application of that program to a subset of available SETA data to illustrate typical wave characteristics for geomagnetically quiet and disturbed periods; and (3) An analysis of the average magnetic activity dependence of high-latitude thermospheric winds and densities below 200 km. These efforts are outlined in the following sections of this report. The first two are reported in published articles and reports, and so the results are presented here in very abbreviated form. The results of effort (3) are not available in published form, and consequently are expanded on in somewhat greater depth in this report. Section 5 summarizes a variety of other efforts performed under Contract F19628-85-k-0041.

2. SIMULATION AND ANALYSIS OF CDAW-6 EVENT

The thermospheric response to the magnetic storm occurring on March 22, 1979, was simulated in collaboration with Dr. R. G. Roble on the NCAR (National Center for Atmospheric Research) TGCM (Thermosphere General Circulation Model) , and compared to the actual response as depicted by winds and densities measured by a satellite-borne accelerometer and ground-based incoherent scatter radar at Millstone Hill. There were three isolated substorms on March 22, 1979, the first starting at about 1054 UT, and the others near 1436 UT and 1800 UT. The primary responsibilities of the P.I. in this project were to specify the electrodynamic and particle precipitation inputs for the TGCM as a function of time during this period, and to perform an interpretive analysis of the observational data and the model results, as outlined in the following.

Results of the TGCM simulation may be found in:

> "Thermospheric Dynamics during the March 22, 1979, Magnetic Storm 1. Model Simulations" by R.G. Roble, J.M. Forbes, and F.A. Marcos, *J. Geophys. Res., 92,* 6045-6068, 1987.

This simulation required the specification of certain parameters which defined the plasma convection pattern and auroral precipitation pattern as a function of time during the event. The cross-cap potential as determined from an empirical formula using IMP-8

IMF data as input were obtained by the P.I. from Dr. P. Reiff of Rice University. The P.I. worked with Dr. Moshe Harel of the Jet Propulsion Laboratory to obtain a numerical simulation of the plasma convection pattern for March 22, 1979, with these cross-cap potentials and the measured AE indices as input. The Rice Convection model was used for this simulation. The parameters for the Heelis empirical plasma convection pattern as utilized in the TGCM were then obtained by fitting the shape of the convection pattern from the Rice model at hourly intervals. Such parameters included the cross-cap potential difference, the convection pattern reversal boundary, latitudinal extent of the convection cells, offset of the flow pattern from the geomagnetic pole, width of the dayside throat region, among other features.

Related efforts concentrated on the input of particle energy into the auroral oval. The data utilized correspond to electron detectors onboard the DMSP F-2 and P78-1 satellites, provided by Dr. David Hardy of AFGL. These data were analyzed for the parameters necessary to meet the functional requirements of the TGCM. These are as follows: auroral oval half-width, average particle energy at the center of the oval, and energy flux at the center of the oval, all at magnetic local noon and magnetic local midnight, as a function of universal time during March 22, 1979. Analytic expressions in the TGCM utilize these quantities to define the full spatial distribution of particle heating.

The TGCM was run using the above parameterizations of the electrodynamic and particle precipitation inputs, and the CHIU model for the ionospheric plasma densities, and history files of the various neutral atmospheric parameters were recorded for every 20 minutes during the event. The TGCM was also run with time-independent, prestorm level aurora and magnetospheric convection forcings so that difference fields of storm time response phenomena could be derived. The enhanced high-latitude energetic inputs during the CDAW-6 interval caused large disturbances in the high latitude circulation, temperature and compositional patterns. They also produced large-scale disturbances that propagate to equatorial latitudes and generally disturb the global circulation, temperature, and composition structure of the upper and lower thermosphere. In the upper thermosphere the high-latitude neutral winds generally followed the two-cell pattern of magnetospheric convection with a lag of only 1/2 - 1 hour. Wind velocities near the peak of the event exceeded 1000 m/sec within the polar cap. Joule heating near the throat of the magnetospheric convection pattern caused the neutral temperature to increase to nearly 2500 K in a localized region, with a more uniform increase of 300 - 500 K over the entire polar cap. The thermospheric response in the northern hemisphere was larger than that generated in the southern hemisphere, primarily because the magnetospheric convection pattern in the northern hemisphere was in sunlight during the storm pe-

riod whereas it was in darkness in the southern hemisphere. The disturbances launched in both auroral zones propagated equatorward, reaching the vicinity of the equator in about 2 hours. At equatorial latitudes there appeared alternating regions of high and low temperatures that resulted because of interacting wave dynamics. As waves converge, adiabatic heating caused by sinking motions increases the temperature; as they diverge, cooling by upward motions decreases the temperature. The equatorward propagating disturbances interact at the equator and develop a poleward propagating component that, in turn, can interact with the next substorm-launched disturbance, etc.

In the lower thermosphere the response is smaller than at F-region heights, and the major variations are confined to high latitudes. There are some equatorward propagating disturbances in the lower thermosphere, but these are primarily associated with the large substorm near 1500 UT and are generally damped as they propagate to lower latitudes. The main lower thermospheric warming is caused by adiabatic heating from the mean motions and downward heat conduction from the upper thermosphere.

The calculated TGCM temperature response was compared with storm-time temperature and density responses predicted by the MSIS-83 empirical model (and also SETA densities; see below). The overall magnitudes of the temperature perturbations caused by the storm are similar for the TGCM and MSIS-83 model predictions, especially in the zonal mean. However, there is considerably more structure associated with local regions of intense heating and wave propagation in the TGCM fields that are not accounted for in the MSIS-83 predictions. It is clear that MSIS-83 gives a good "climatological" or mean representation of the storm response whereas the TGCM accounts for time-dependent "weather" processes with a much higher time resolution.

A comparison was made between the TGCM simulations, satellite electrostatic accelerometer (SETA) measurements of neutral (cross-track) winds and total mass densities between 170 and 240 km, and mid-latitude Thomson scatter measurements of neutral exospheric temperatures. Full details of this effort are documented in:

> "Thermospheric Dynamics during the March 22, 1979, Magnetic Storm. 2. Comparisons of Model Predictions with Observations," J.M. Forbes, R.G. Roble, and F.A. Marcos, *J. Geophys. Res., 92,* 6069-6081, 1987.

Briefly, the following points of consistency between theory and observation were noted:

1. A localized region of daytime density enhancement (60% at 180 km) occurred in both the simulation and the data near the throat of the plasma convection pattern.

2. The night sector is generally characterized by more wavelike structures, indicating phase progression toward the equator, horizontal scales of 1500 km, and density perturbations of 20-40%.

3. Polar region winds (normal to the satellite track) occur with velocities of 250-600 m/sec and are consistent with the antisunward and return flows characteristic of a two-cell pattern similar to that of the convecting ions, but rotated several hours later in local time.

Points of departure between theory and observation:

1. The TGCM "hot spot" extends much farther into the nighttime sector (down to about 60° latitude) than is consistent with the SETA measurements (no less than 75° latitude), possibly indicating incorrect positioning, orientation, or latitudinal extent of the convection pattern in the TGCM.

2. Reversals to eastward winds of 200-300 m/sec are measured in the prenoon sector below 60° latitude, consistent with what one would expect from a strong return flow, whereas the TGCM winds are weak (less than 100 m/sec) and westward at the same time and location.

3. The measurements also indicate a shift to eastward winds (roughly 200 m/sec) in the premidnight sector below 50° latitude, implying a sharp transition from convection-driven to EUV-driven winds. While the observed wind directions below 50° latitude are consistent with the EUV-driven diurnal tide, the amplitudes are about twice what one would normally expect.

The reversals referred to in points 2 and 3 above are also evident in other wind and ion drift measurements during disturbed times, as noted by Forbes et al. [1987]. These discrepancies may be explicable in part by erroneous positioning, latitudinal extent, or orientation of the driving convection pattern in the TGCM. Recall that the convection pattern was made to be consistent with simulations provided by the Rice University convection model by appropriately choosing the adjustable parameters in the Heelis empirical model. One possibility is that there are IMF-By effects in the convection pattern that are not taken into account in this formulation but which bear relevance to point 2 above. For instance, ion convection patterns based on Dynamics Explorer 2 data show distortions in the daytime throat region which would result in flow reversals in the prenoon sector similar to that observed by the SETA instrument.

Concerning point 3 above, a convection pattern which covers a more restricted geographical region (that is, does not extend as far down in latitude) would not only yield a shift to eastward nighttime winds as observed in the wind data, but would also be consistent with the noted discrepancies between measured and simulated densities (point 1 above). Forbes et al. [1987] speculate that the occurrence of enhanced eastward winds before midnight may be connected with a raising of the F layer by the southward 'midnight surge', thus diminishing the decelerating force on the eastward wind component.

3. SPECTRAL/WAVE ANALYSIS OF SETA DENSITIES

A computerized procedure was developed for spectrally analyzing SETA density data using the Maximum Entropy Method (MEM), and applied to typical quiet and magnetically active days during July 1983 to demonstrate the methodology, and provide a preliminary assessment as to the magnetic activity dependence of wave occurrences and characteristics. The complete spectral/wave analysis effort is documented in:

> "Wave Structures in Thermospheric Density from Satellite Electrostatic Triaxial Accelerometer Measurements," J.M. Forbes, F.A. Marcos, and P.F. Fougere, AFGL Report AFGL-TR-87-0189, June, 1987, ADA194134.

This report provides

1. A brief history of wave analyses of thermospheric data and a summary of theoretical results.

2. A description of the pre-processing of SETA data, including sampling filtering, and geophysical sorting.

3. Documentation of a procedure to use existing FORTRAN programs, appropriately modified for the specialized purposes at hand, which were developed by Dr. Paul Fougere, to produce de-trended data and spectral plots.

4. A review of spectral analysis by the Maximum Entropy Method (MEM) as it applies to the SETA data analyzed.

5. A preliminary analysis of the spectral results as a function of local time and geomagnetic activity.

The conclusions of this latter interpretive analysis are as follows:

1. Wave motions contribute to the observed variability of density during both quiet and active conditions, and become increasingly important as magnetic disturbances become more intense.

2. There exists evidence for enhanced wave activity at high latitudes and during nighttime.

3. There exists a significantly higher probability of finding waves of horizontal wavelengths between 1250-2000 km and 150-500 km, especially during geomagnetically disturbed conditions, as opposed to those waves with wavelengths between 500 and 1250 km. The former, larger-scale, waves are known to be capable of propagating large distances with little attenuation. It is tentatively concluded that the relatively frequent occurrence of the shorter-scale waves, even at low latitudes, may be attributable to ducting in the lower thermosphere which allows them to travel large distances as suggested in the recent literature by H.G. Mayr and colleagues.

These preliminary findings can be verified and further refined through analysis of additional satellite density data now in existence. The above report provides a computerized procedure to process these data to reveal the dominant wave characteristics, and a rationale and direction for future scientific efforts along these lines.

4. AVERAGE MAGNETIC ACTIVITY DEPENDENCE OF HIGH-LATITUDE THERMOSPHERIC WINDS AND DENSITIES BELOW 200 KM

4.1 SETA Winds and Densities vs. Kp*

The main findings of this paper are summarized in Figure 1. Here the bin-averaged (a) daytime (~1030 LT) cross-track wind (positive to the east) component (Figure 1a), (b) nighttime (~2130 LT) cross-track wind component (Figure 1b), (c) daytime density and (d) nighttime density, are plotted vs. geomagnetic latitude (45-90°) and Kp*, the Kp-index average for the 3-hour period containing the measurement with that of the previous 3-hour period. Figures 2a and 2b represent line plots corresponding to Figures 1a and 1b for quiet and active magnetic conditions wherein the Kp-binning has been performed in one-unit bins of Kp. In the interpretation of these data it is important to note that because the orbit is not strictly polar, the angle between the zonal wind component and the satellite cross-track direction is a function of geographic latitude. As the geographic pole is approached, the component of measured cross-axis wind shifts from mainly zonal toward meridional. Furthermore, the reference direction for the cross-track wind is such that for the upleg (daytime) data, negative (positive) values correspond

to the eastward (westward) component of the wind vector below about 70° latitude, and to the southward/eastward (northward/westward) component at higher latitudes; whereas, for the downleg (nighttime) data, negative (positive) values correspond to the westward (eastward) component of the wind vector below about 70° latitude, and to the southward/westward (northward/eastward) at high latitudes.

Turning now to Figures 1a and 2a, the daytime winds are characterized by an eastward flow regime (~100 ms-1) below about 70° magnetic latitude under quiet geomagnetic conditions, which intensifies (to ~ 200 ms-1) and whose upper latitude limit decreases to about 65° for Kp*'s in excess of 3 to 4. At higher latitudes, the westward/northward component of the flow typically increases in amplitude from 100 to 350 ms-1 as magnetic activity increases. In the night sector (Figures 1b and 2b), the northward/eastward component of the flow exhibits a similar increase with magnetic activity. The lower boundary of this flow regime occurs at about 70° magnetic latitude for all levels of magnetic activity. At lower latitudes the transition is to a westward-oriented flow and then back again to an eastward orientation, this transition occurring at progressively lower latitudes (from 60° to 45°) as Kp* increases from 0-2 to 5-7, accompanied by an intensification of the westward flow regime from 50-75 ms-1 to 150-200 ms-1. Although the satellite only senses cross-track winds, precluding a unique determination of the flow pattern, the above characteristics are consistent with the familiar two-cell high-latitude flow pattern with antisunward flow over the pole and return flows in the dawn and dusk sectors, covering an expanded geographical area and consisting of more intense winds as magnetic activity increases.

Figures 1c and 1d illustrate average densities (normalized to 200 km) vs. geomagnetic latitude and Kp*. There is a general trend for increased densities with enhanced geomagnetic activity, but this trend is not smooth and is not characterized by any clear dependences on latitude or local time. The corresponding line plots in Figure 3, which correspond to binning in whole units of Kp*, do however, with few exceptions, increase monotonically with Kp*.

4.2 SETA Winds vs. Kp, Phi, ln AE, Phi*

Figures 1, 2, and 3, and specifically the choice of Kp* as the adopted geophysical parameter, represent the end result of a comprehensive statistical analysis of the SETA data. Initially, day and night data were each segmented into geomagnetic latitude bins 45-50°, 55-65°, 65-75° and linear regression analyses performed for each bin with various indices and time delays. The indices utilized included the Kp index for the three-hour period containing the SETA measurement, the average of Kp and its previous value (Kp*), the

log of the auroral electrojet index (AE), the hourly cross-cap potential Phi as determined from IMF data using the Reiff empirical formula, and the average of Phi (Phi*) for the three hours preceding the density or wind measurement. While it was not unusual for the correlation coefficients (R) corresponding to density to occur in the .80-.95 range, R-values for winds were often less than 0.6, indicating that less than 36% (R squared) of the variability was being modeled. This led us to perform binning and averaging of the data to enable plots such as those presented in Figure 4, which are typical of our study, to be produced. These plots indicate the mean trends in the data to be nonlinear and/or non-monotonic, both features of which contribute to the lack of correlation between the winds and any one of these geophysical parameters. In addition, the large standard deviations associated with the bin-averaged winds greatly reduce the quality of fit of any regression equation. Standard deviations corresponding to the mean values given in Figure 4, which typify results for other latitudes, local times, and indices we have considered, are given in Table 1. As the standard deviations are often as large as the mean wind values, confident quantitatively statistical relationships are thus impossible to obtain. The curves in Figure 4 furthermore indicate the magnetic activity indices to be strongly correlated with each other, such that no one of them should be expected to vastly outperform the others in terms of density and wind predictability. There was, however, a small margin of improved behavior for Kp* in terms of correlation coefficient, monotonicity, and consistency. It was this index, therefore, that was adopted for displaying the data in Figures 1, 2, and 3. The variations of dayside and nightside winds in three latitude bins are illustrated in Figure 5 for Kp* and Figure 6 for Phi*.

5. OTHER EFFORTS

The following manuscript was prepared for presentation and inclusion in the printed proceedings of the Workshop on Atmospheric Density and Aerodynamic Drag Models for Air Force Operations, AFGL, 20-22 October, 1987:

"Mesosphere-Thermosphere Coupling", by J.M. Forbes

This paper reviewed the basic processes and physical mechanisms thought to govern the dynamical and thermal structure of the 80 - 150 km height region, provided an assessment of current research in the field, and identified areas where future research areas should be directed. The paper provided much emphasis on atmospheric tidal oscillations in the region, the density perturbations associated with tides, and a methodology by which radar observations of tides can be used in combination with theory to provide oscillating lower boundary conditions for TGCMs.

At the request of the Air Force, the following unpublished report was prepared:

> "Density Variability and Recommendations for Achieving Improved Density Specifications between 60 and 150 km," by J.M. Forbes, unpublished report.

This report provided estimates of density variability due to gravity waves, tides, and secular variations, made recommendations for achieving an improved capability for making density predictions in the region, and in addition, made some estimates of achievable improvements over current capabilities to specify atmospheric density. As an extension and supplement to the climatological study described in Section 4, and as a result of the recognition of the importance of thermosphere-ionosphere interactions in the study described in Section 2, a second, more extended period of enhanced geomagnetic activity, March 25-29, 1979, was examined from the point of view of comparing global ionospheric data with the SETA winds and densities. The ionosonde data consist of foF2, hmF2, "effective" meridional winds inferred from hmF2, and 24-hour averages of the effective winds. Color figures (slides and photos) were produced which compare these parameters, in particular the latitudinal penetration of magnetic activity-enhanced features, with those in the SETA density and wind data. Phenomena such as the midnight surge and storm negative phase effect are interpretable in terms of neutral-plasma interactions during this period of enhanced geomagnetic activity. Further support is being sought to complete the analysis of this data and prepare a manuscript for publication.

REFERENCES

"Thermospheric Dynamics during the March 22, 1979, Magnetic Storm 1. Model Simulations" by R.G. Roble, J.M. Forbes, and F.A. Marcos, *J. Geophys. Res., 92,* 6045-6068, 1987.

"Thermospheric Dynamics during the March 22, 1979, Magnetic Storm. 2. Comparisons of Model Predictions with Observations," J.M. Forbes, R.G. Roble, and F.A. Marcos, *J. Geophys. Res., 92,* 6069-6081, 1987.

"Wave Structures in Thermospheric Density from Satellite Electrostatic Triaxial Accelerometer Measurements," J.M. Forbes, F.A. Marcos, and P.F. Fougere, AFGL Report AFGL-TR-87-0189, June, 1987, ADA194134.

"Mesosphere-Thermosphere Coupling", J.M. Forbes, Proc. Workshop on Atmospheric Density and Aerodynamic Drag Models for Air Force Operations, AFGL, 20-22 October, 1987.

TABLE 1

AVERAGE DAYSIDE CROSS-TRACK WINDS (ms^{-1}) AND DENSITIES (gcm^{-3}) FOR 45° - 55° AND 65° - 75° MAGNETIC LATITUDE BINS WITH STANDARD DEVIATIONS AND #PTS/BIN, VS. AVERAGE POLAR CAP POTENTIAL AND Kp AS DEFINED IN TEXT.

	45° - 55°					65° - 75°				
	#PTS	WIND	σ	DENSITY	σ	#PTS	WIND	σ	DENSITY	σ
Φ = 0-30	29	114	76	.36	.018	32	-18	89	.35	.017
30-60	99	83	109	.37	.020	102	-28	100	.35	.026
60-90	90	46	131	.39	.027	93	-53	123	.37	.041
90-120	64	10	134	.39	.025	69	-20	127	.37	.045
120-150	21	-56	150	.41	.024	24	-95	124	.39	.039
150-180	9	-115	169	.43	.020	10	-100	229	.42	.034
180-210	4	-196	133	.45	.035	4	-28	338	.40	.019
Kp= 0-1	9	145	105	.36	.015	12	22	92	.35	.011
1-2	62	116	68	.36	.018	63	-30	94	.34	.016
2-3	84	77	89	.37	.019	89	-37	123	.35	.021
3-4	93	64	118	.39	.022	99	-29	115	.37	.032
4-5	41	-18	156	.40	.029	43	-72	111	.58	.032
5-6	27	-76	154	.41	.024	28	-11	142	.38	.040
6-7	13	-169	143	.41	.032	15	-123	168	.40	.044
7-8	4	-174	109	.45	.030	4	1	337	.41	.065

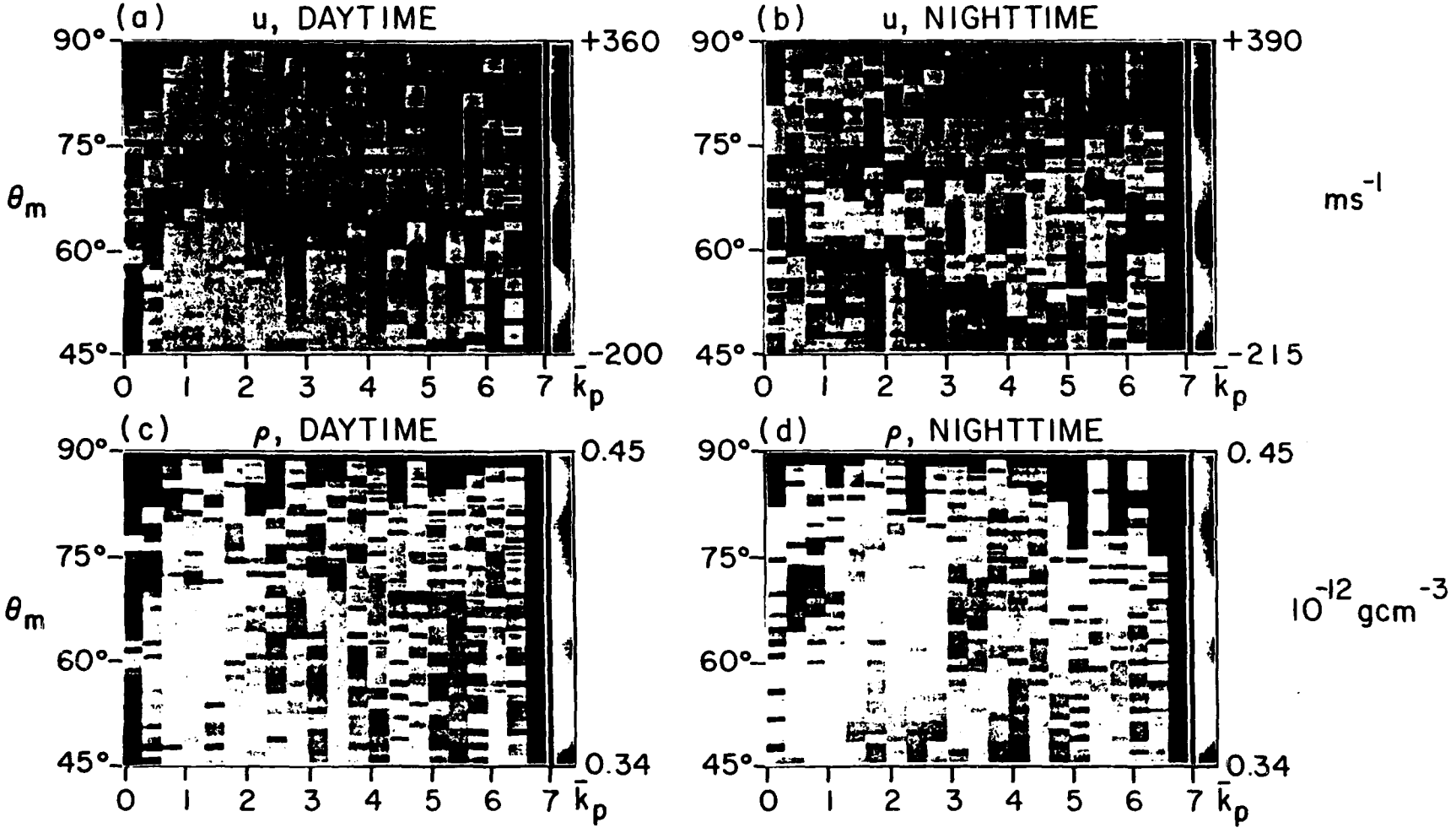
(a) u, DAYTIME
(b) u, NIGHTTIME
(c) ρ, DAYTIME
(d) ρ, NIGHTTIME
90°
75°
60°
45°
θm
0 1 2 3 4 5 6 7 k̄p
+360
-200
+390
-215
ms-1
0.45
0.34
10-12 gcm-3

Figure 1

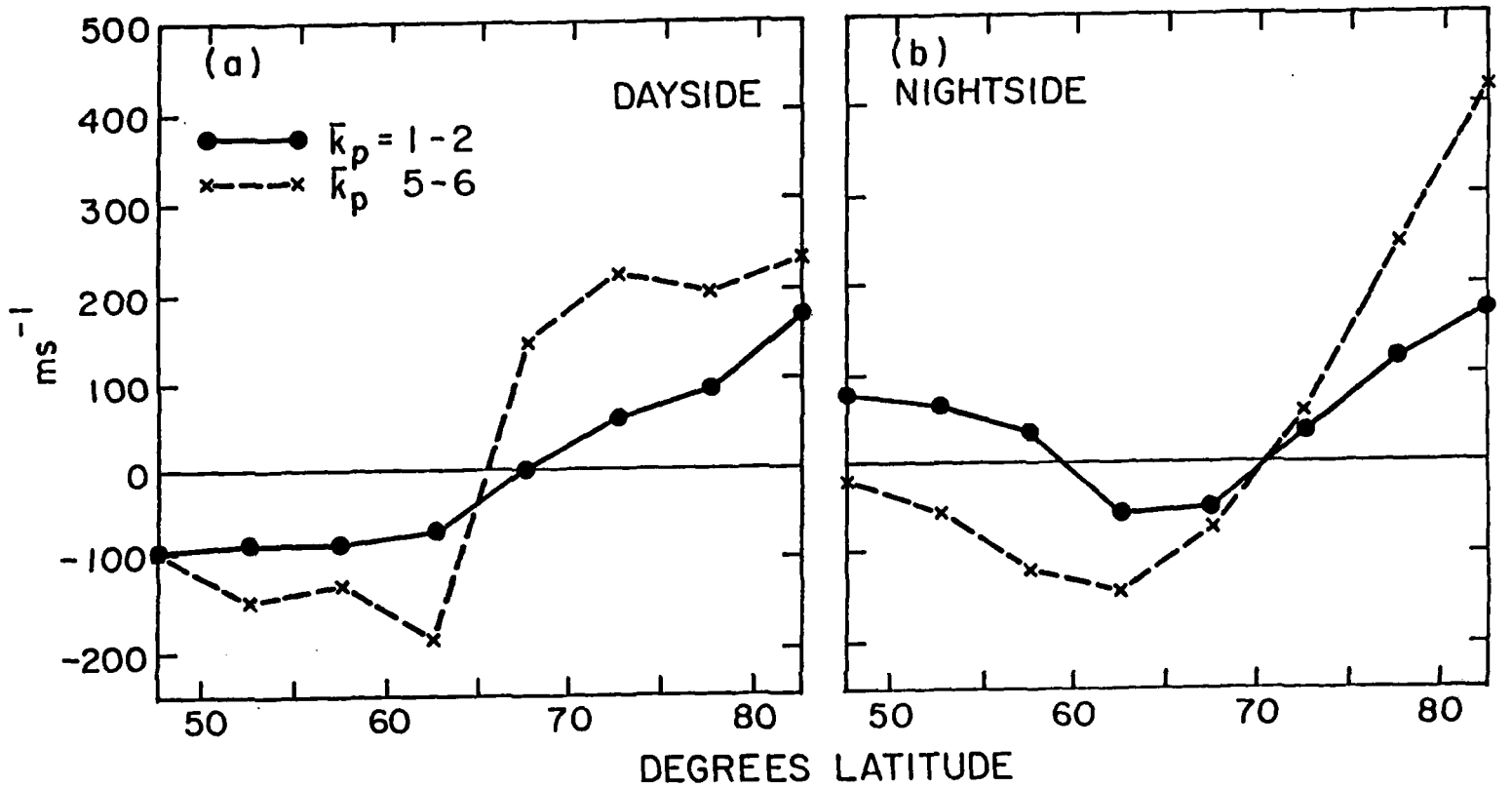
(a)
DAYSIDE
$\bar{k}_p$ = 1-2
$\bar{k}_p$ 5-6
(b)
NIGHTSIDE
500
400
300
200
100
0
-100
-200
ms^{-1}
50
60
70
80
DEGREES LATITUDE

Figure 2

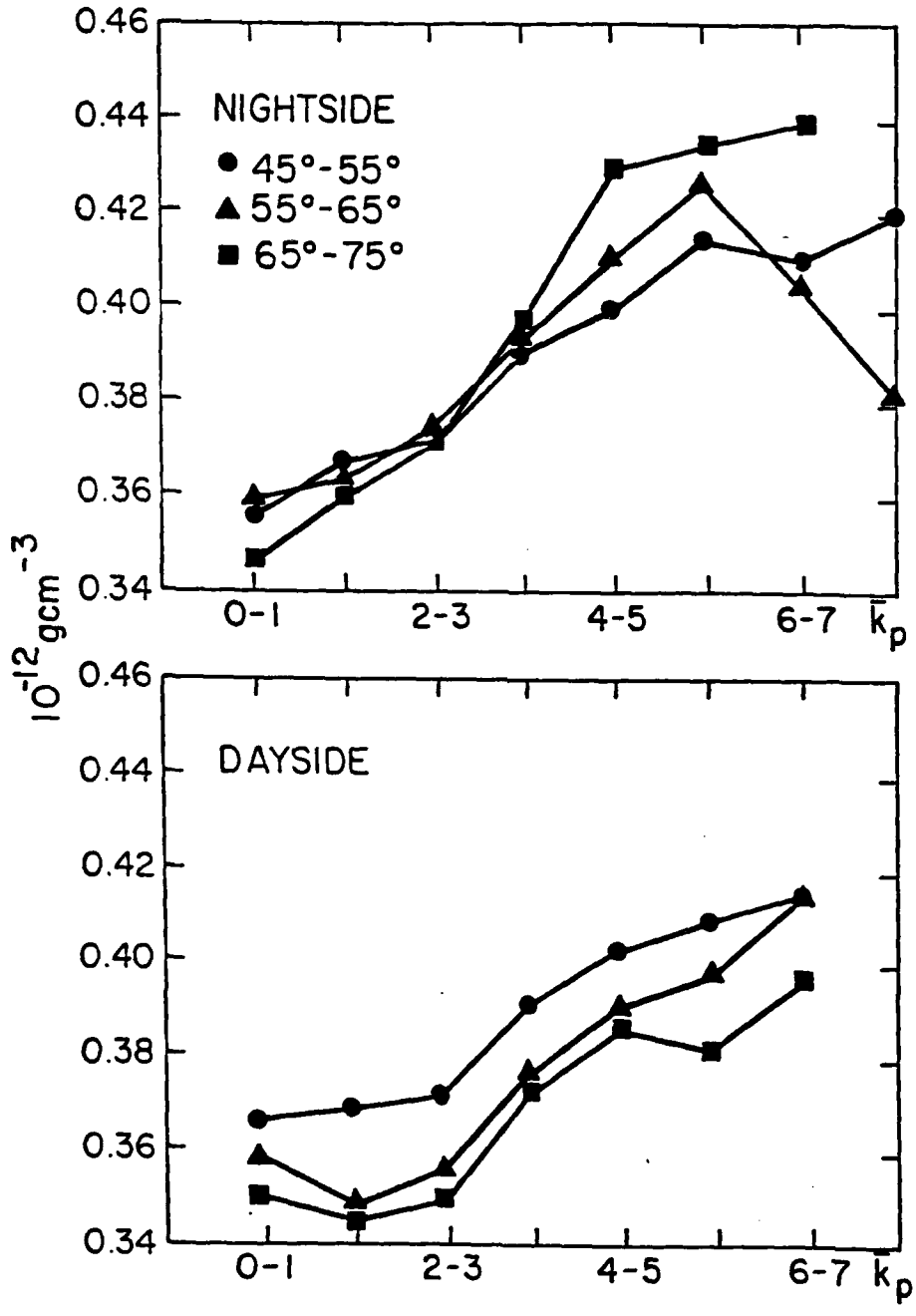
NIGHTSIDE
45°-55°
55°-65°
65°-75°
DAYSIDE
0.46
0.44
0.42
0.40
0.38
0.36
0.34
0-1
2-3
4-5
6-7
$\bar{k}_p$
10^{-12} gcm^{-3}

Figure 3

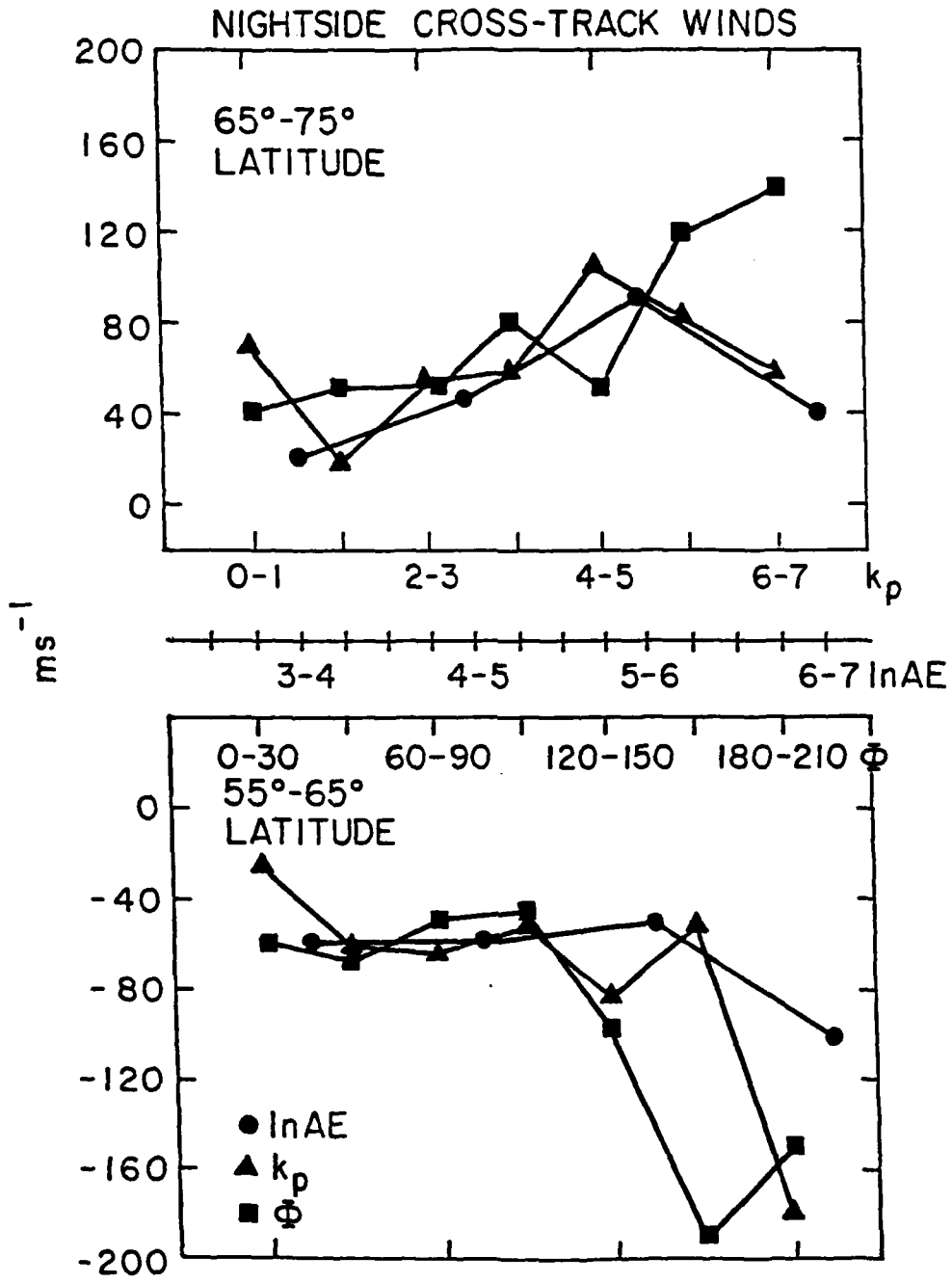
NIGHTSIDE CROSS-TRACK WINDS
65°-75°
LATITUDE
200
160
120
80
40
0
0-1
2-3
4-5
6-7
k_p
ms^{-1}
3-4
4-5
5-6
6-7 InAE
0-30
60-90
120-150
180-210 Φ
55°-65°
LATITUDE
0
-40
-80
-120
-160
-200
● InAE
▲ k_p
■ Φ

Figure 4

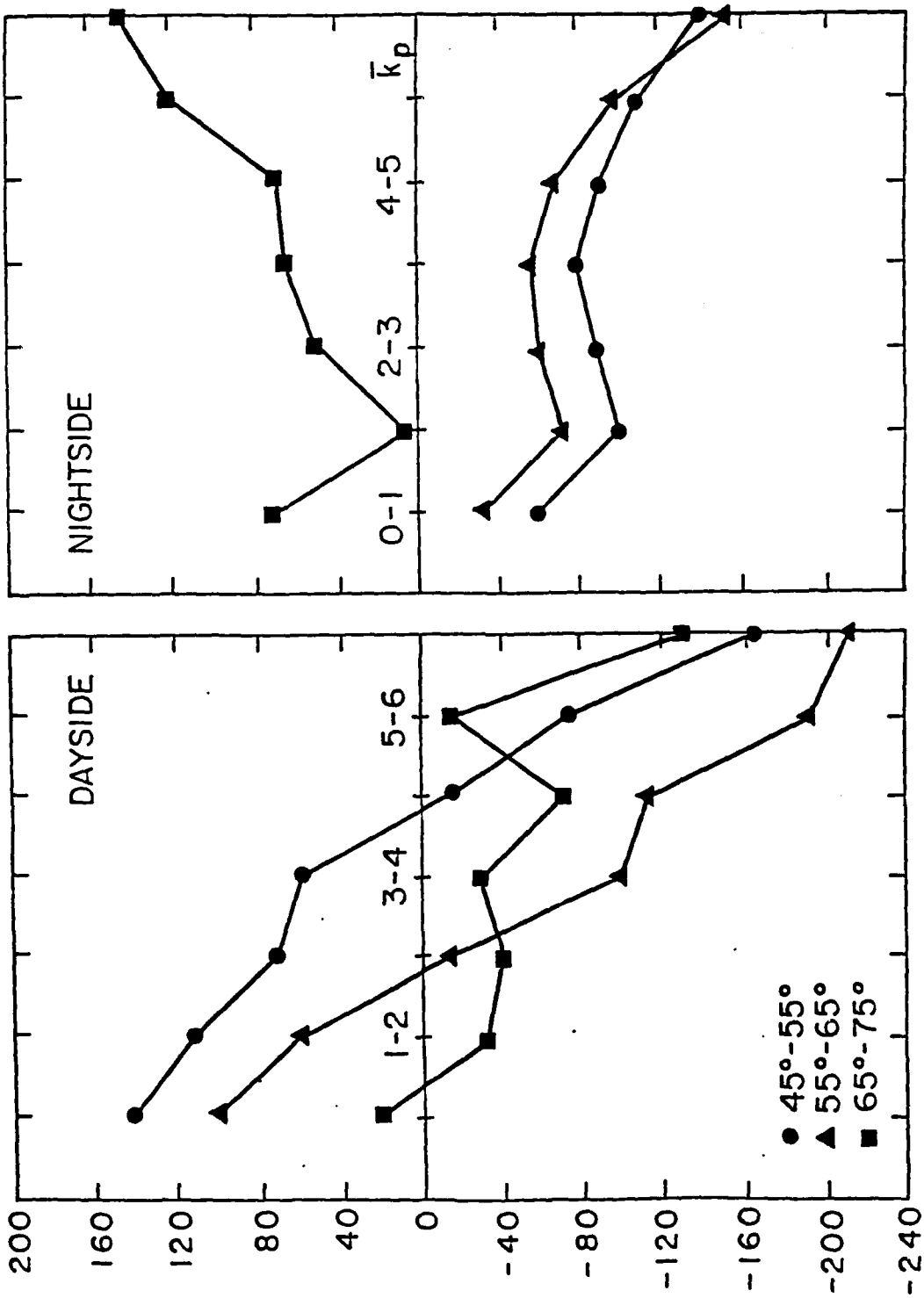
NIGHTSIDE
DAYSIDE
0-1
2-3
4-5
1-2
3-4
5-6
$\bar{k}_p$
● 45°-55°
▲ 55°-65°
■ 65°-75°
200
160
120
80
40
0
-40
-80
-120
-160
-200
-240

Figure 5

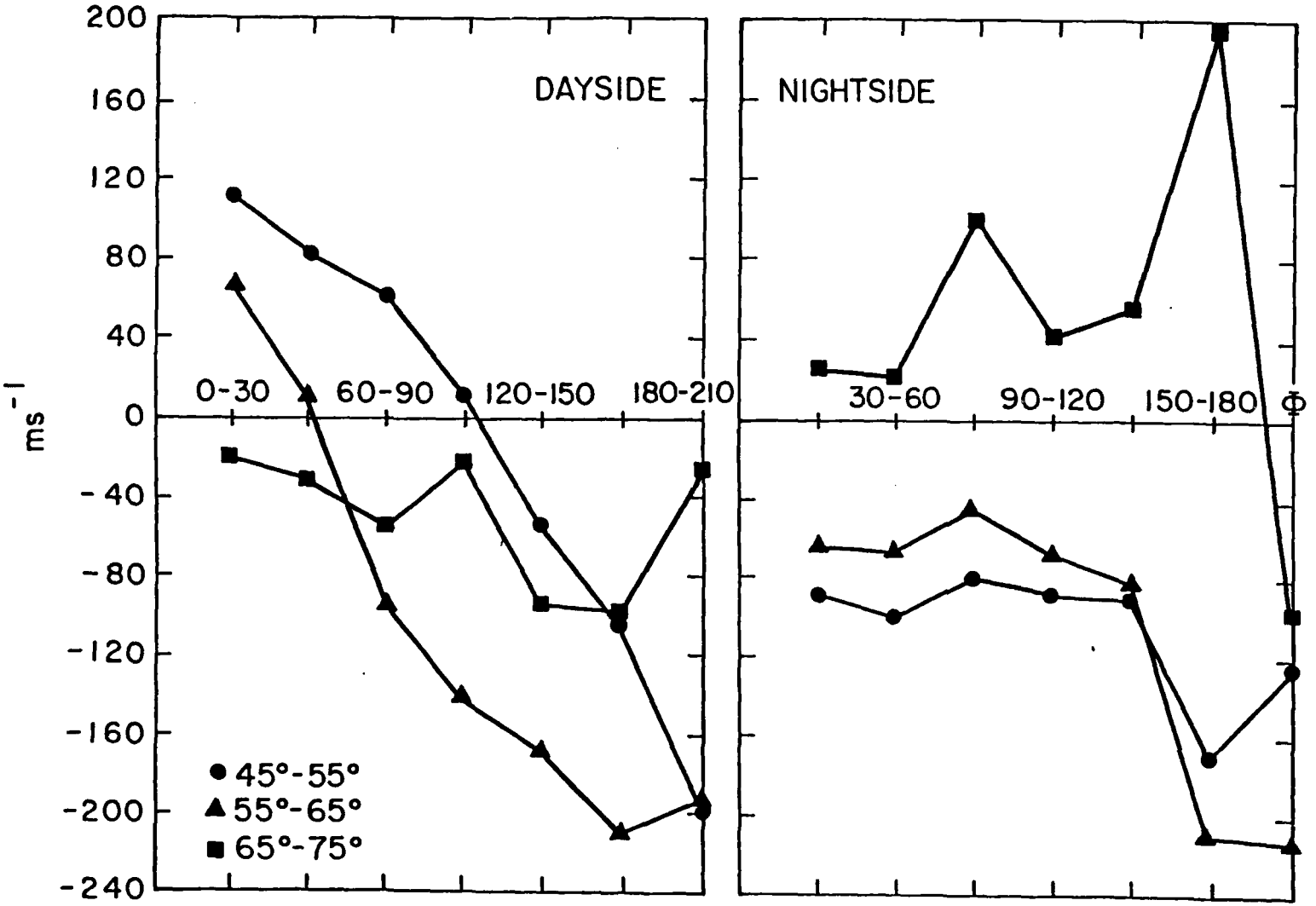
200
160
120
80
40
0
-40
-80
-120
-160
-200
-240
ms⁻¹
DAYSIDE
NIGHTSIDE
0-30
60-90
120-150
180-210
30-60
90-120
150-180
Φ
● 45°-55°
▲ 55°-65°
■ 65°-75°

Figure 6